Long-Wave Anisotropic Behavior of Highly Heterogeneous Fractured Biot Media

Juan E. Santos[123] – Robiel Martínez Corredor[3]

[1] Instituto del Gas y del Petróleo, Facultad de Ingeniería, Universidad de Buenos Aires.

[2] Department of Mathematics, Purdue University

[3] Universidad Nacional de la Plata

SEG INTERNATIONAL EXPOSITION AND 87TH ANNUAL MEETING
HOUSTON•TEXAS
24-29 SEPTEMBER 2017

Introduction.I

- Fast compressional or shear waves travelling through a fluid-saturated porous material (a Biot medium) containing heterogeneities on the order of centimeters (mesoscopic scale) suffer attenuation and dispersion observed in seismic data.
- Since extremely fine meshes are needed to represent these type of mesoscopic-scale heterogeneities, numerical simulations are very expensive or not feasible.

Introduction.II

- Alternative: In the context of Numerical Rock Physics, perform compressibility and shear time-harmonic experiments to determine a long-wave equivalent viscoelastic medium to a highly heterogeneous Biot medium.
- This viscoelastic medium has in the average the same attenuation and velocity dispersion than the highly heterogeneous Biot medium.

SEG INTERNATIONAL EXPOSITION AND 87TH ANNUAL MEETING
HOUSTON•TEXAS
24-29 SEPTEMBER 2017

Introduction.III

- Each experiment is associated with a Boundary Value Problem (BVP) that is solved using the Finite Element Method (FEM).

The basic concepts and ideas used in this presentation can be found in the book

Numerical Simulation in Applied Geophysics

by Juan Santos and Patricia Gauzellino, Birkhauser, 2016

SEG INTERNATIONAL EXPOSITION AND 87TH ANNUAL MEETING
HOUSTON·TEXAS
24-29 SEPTEMBER 2017

Biot's Equations in the Diffusive Range of Frequencies.I

- Frequency-domain stress-strain relations in a Biot medium

$$\sigma_{st}(\mathbf{u}) = 2G^{(\theta)}e_{st}(\mathbf{u}_s) + \delta_{st}\left(\lambda_U^{(\theta)}\nabla\cdot\mathbf{u}_s - \alpha^{(\theta)}M^{(\theta)}\xi\right),$$

$$p_f(\mathbf{u}) = -\alpha^{(\theta)}M^{(\theta)}\nabla\cdot\mathbf{u}_s + M^{(\theta)}\xi, \qquad \theta = b, f.$$

where $\mathbf{u} = (\mathbf{u_s}, \mathbf{u}_f)$, $\mathbf{u}_s = (\mathbf{u}_{s,1}, \mathbf{u}_{s,3})$, $\mathbf{u_f} = (\mathbf{u}_{f,1}, \mathbf{u}_{f,3})$ and e_{st} is the strain tensor at the mesoscale.

Biot's Equations in the Diffusive Range of Frequencies.II

- Biot's equations in the diffusive range:

$$\nabla \cdot \boldsymbol{\sigma}(\mathbf{u}) = 0,$$

$$\frac{\mathrm{i}\omega\mu^{(\theta)}}{\kappa^{(\theta)}}\mathbf{u}_f + \nabla p_f(\mathbf{u}) = 0,$$

where μ is the fluid viscosity, κ is the frame permeability.

Boundary Conditions at a Fracture within a Biot Medium.I

- Consider a rectangular domain $\Omega = (0, L_1) \times (0, L_3)$ with boundary Γ in the (x_1, x_3)- plane, with x_1 and x_3 being the horizontal and vertical coordinates, respectively.
- Ω contains a set of $J^{(f)}$ horizontal fractures $\Gamma^{(f,l)}$, $l = 1, \cdots, J^{(f)}$ each one of length L_1 and aperture $h^{(f)}$. This set of fractures divides Ω in a collection of non-overlapping rectangles $R^{(l)}$,

Boundary Conditions at a Fracture within a Biot Medium.II

- Assume that the rectangles $R^{(l)}$ and $R^{(l+1)}$ have a fracture $\Gamma^{(f,l)}$ as a common side.
- Let $[\mathbf{u}_s]$, $[\mathbf{u}_f]$ denote the jumps of the solid and fluid displacement vectors at $\Gamma^{(f,l)}$, i.e.

$$[\mathbf{u}_s] = \left(\mathbf{u}_s^{(l+1)} - \mathbf{u}_s^{(l)}\right)\Big|_{\Gamma^{(f,l)}}$$

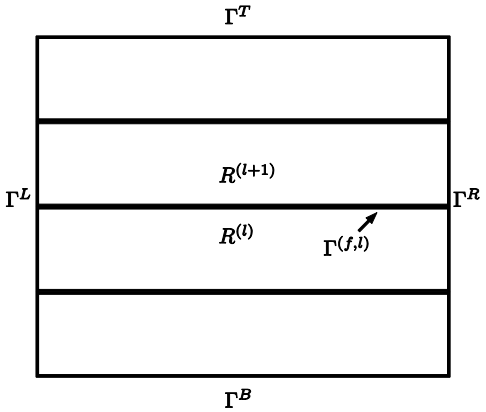

Boundary Conditions at a Fracture within a Biot Medium.III

- $\nu_{l,l+1}$ and $\chi_{l,l+1}$: the unit outer normal and a unit tangent (oriented counterclockwise) on $\Gamma^{(f,l)}$ from $R^{(l)}$ to $R^{(l+1)}$.
- $\left[\mathbf{u}_s \cdot \boldsymbol{\nu}_{l,l+1}\right] =$

$$\eta_N \left(\left(1 - \alpha^{(f)} \tilde{B}^{(f)} (1 - \Pi)\right) \boldsymbol{\sigma}(\mathbf{u}) \nu_{l,l+1} \cdot \boldsymbol{\nu}_{l,l+1} - \alpha^{(f)} \frac{1}{2} \left(\left(-p_f^{(l+1)}\right) + \left(-p_f^{(l)}\right) \right) \Pi \right),$$

$$\Gamma^{(f,l)},$$

Boundary Conditions at a Fracture within a Biot Medium.IV

- $\left[\mathbf{u}_s \cdot \boldsymbol{\chi}_{l,l+1}\right] = \eta_T \boldsymbol{\sigma}(\mathbf{u}) \nu_{l,l+1} \cdot \boldsymbol{\chi}_{l,l+1}, \quad \Gamma^{(f,l)},$
- $\left[\mathbf{u}_f \cdot \boldsymbol{\nu}_{l,l+1}\right] =$

$$\alpha^{(f)} \eta_N \left(\boldsymbol{\sigma}(\mathbf{u}) \nu_{l,l+1} \cdot \boldsymbol{\nu}_{l,l+1} + \frac{1}{\tilde{B}^{(f)}} \frac{1}{2} \left(\left(-p_f^{(l+1)} \right) + \left(-p_f^{(l)} \right) \right) \right) \Pi, \quad \Gamma^{(f,l)},$$

Boundary Conditions at a Fracture within a Biot Medium.V

- $\left(-p_f^{(l+1)}\right) - \left(-p_f^{(l)}\right) = \frac{\mathrm{i}\omega\mu^{(f)}\Pi}{\hat{\kappa}^{(f)}} \frac{1}{2}\left(\mathbf{u}_f^{(l+1)} + \mathbf{u}_f^{(l)}\right) \cdot \boldsymbol{\nu}_{l,l+1}, \quad \Gamma^{(f,l)},$
- $\sigma(\mathbf{u})\nu_{l,l+1} \cdot \nu_{l,l+1} = \sigma(\mathbf{u})\nu_{l+1,l} \cdot \nu_{l+1,l},$
- $\sigma(\mathbf{u})\nu_{l,l+1} \cdot \chi_{l,l+1} = \sigma(\mathbf{u})\nu_{l+1,l} \cdot \chi_{l+1,l},$
- η_N and η_T are the fracture normal and tangencial compliances

Boundary Conditions at a Fracture within a Biot Medium.VI

- The fracture dry plane wave modulus $H_m^{(f)} = K_m^{(f)} + \frac{4}{3}G^{(f)}$ and the dry fracture shear modulus $G^{(f)}$ are defined by the relations $\eta_N = \frac{h^{(f)}}{H_m^{(f)}}$, $\eta_T = \frac{h^{(f)}}{G^{(f)}}$,
- $h^{(f)}$ is the fracture aperture and $\hat{\kappa}^{(f)} = \frac{\kappa^{(f)}}{h^{(f)}}$

Boundary Conditions at a Fracture within a Biot Medium.VII

- $\epsilon = \frac{(1+\mathrm{i})}{2}\left(\frac{\omega\mu^{(f)}\alpha^{(f)}\eta_N}{2\widetilde{B}^{(f)}\hat{\kappa}^{(f)}}\right)^{1/2}$, $\Pi(\epsilon) = \frac{\tanh(\epsilon)}{\epsilon}$, $\widetilde{B}^{(f)} = \frac{\alpha^{(f)}M^{(f)}}{H_U^{(f)}}$.

The Equivalent TIV Medium.I

- A Biot medium with a dense set of horizontal fractures behaves as a **Transversely Isotropic and Viscoelastic** (TIV) medium when the average fracture distance is much smaller than the predominant wavelength of the travelling waves.
- Denote by $\tau_{ij}(\tilde{\mathbf{u}}_s)$ and $\epsilon_{ij}(\tilde{\mathbf{u}}_s)$ the stress and strain tensor components of the equivalent TIV medium and by $\tilde{\mathbf{u}}_s$ the solid displacement vector at the macroscale

The Equivalent TIV Medium.II

- $\tau_{11}(\tilde{\mathbf{u}}_s) = p_{11}\epsilon_{11}(\tilde{\mathbf{u}}_s) + p_{12}\epsilon_{22}(\tilde{\mathbf{u}}_s) + p_{13}\epsilon_{33}(\tilde{\mathbf{u}}_s),$
- $\tau_{22}(\tilde{\mathbf{u}}_s) = p_{12}\epsilon_{11}(\tilde{\mathbf{u}}_s) + p_{11}\epsilon_{22}(\tilde{\mathbf{u}}_s) + p_{13}\epsilon_{33}(\tilde{\mathbf{u}}_s),$
- $\tau_{33}(\tilde{\mathbf{u}}_s) = p_{13}\epsilon_{11}(\tilde{\mathbf{u}}_s) + p_{13}\epsilon_{22}(\tilde{\mathbf{u}}_s) + p_{33}\epsilon_{33}(\tilde{\mathbf{u}}_s),$
- $\tau_{23}(\tilde{\mathbf{u}}_s) = 2p_{55}\epsilon_{23}(\tilde{\mathbf{u}}_s),$
- $\tau_{13}(\tilde{\mathbf{u}}_s) = 2p_{55}\epsilon_{13}(\tilde{\mathbf{u}}_s), \qquad \tau_{12}(\tilde{\mathbf{u}}_s) = 2p_{66}\,\epsilon_{12}(\tilde{\mathbf{u}}_s).$

The Equivalent TIV Medium.III

Determination of p_{33}:

$$\frac{\Delta V(\omega)}{V} = -\frac{\Delta P}{p_{33}(\omega)}$$

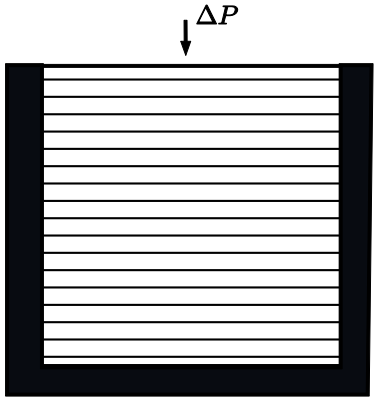

The Equivalent TIV Medium.IV

Determination of p_{11}:

$$\frac{\Delta V(\omega)}{V} = -\frac{\Delta P}{p_{11}(\omega)}$$

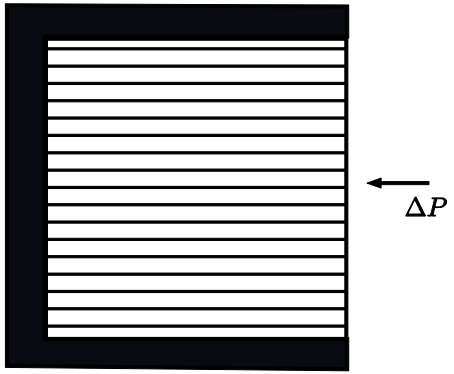

The Equivalent TIV Medium.V

Determination of p_{55}:

$$\tan(\beta_1(\omega)) = \frac{\Delta G}{p_{55}(\omega)}$$

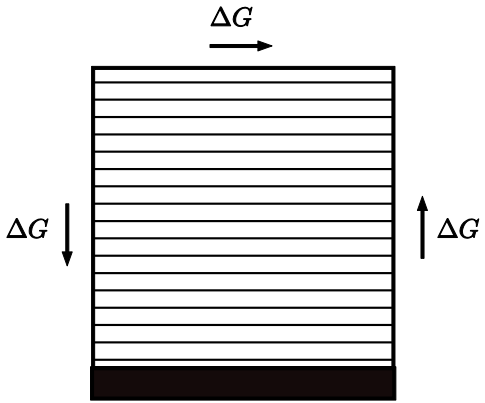

The Equivalent TIV Medium.VI

Determination of p_{66}:

$$\tan(\beta_2(\omega)) = \frac{\Delta G}{p_{66}(\omega)}$$

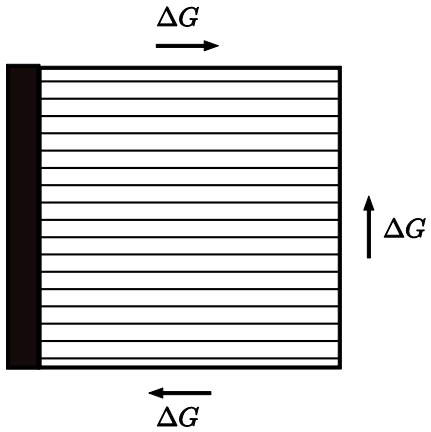

The Equivalent TIV Medium.VII

Determination of p_{13}:

$$p_{13}(\omega) = \frac{p_{11}\epsilon_{11} - p_{33}\epsilon_{33}}{\epsilon_{11} - \epsilon_{33}}$$

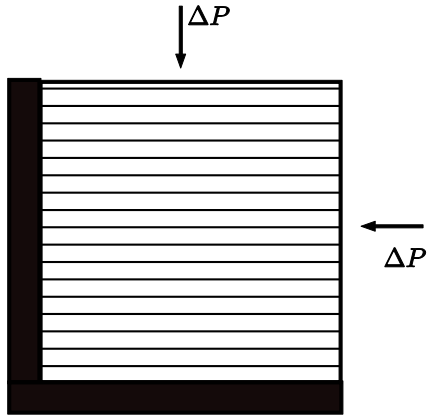

Numerical Experiments.I

- In all the experiments we used square samples of side length 2 m, with 9 fractures at equal distance of 20 cm.
- In the first two experiments, the samples contain Material 1 in the background and Material 2 in the fractures. In the last experiment, both background and fractures contain different proportions of Material 3.

Rock properties			
	Material 1	Material 2	Material 3
K_s (GPa)	36	36	36
ρ_s (Kg/m^3)	2700	2700	2700
ϕ	0.15	0.5	0.65
K_m (GPa)	9.0	0.0055	0.0044
μ (GPa)	7.0	0.0033	0.0022
κ (D)	0.1	10.0	20.0

Numerical Experiments.II

Example 1:

- This experiment validates the results by comparison with those obtained modeling the fractures as very thin layers.
- We consider a brine saturated sample, with brine having density ρ_f= 1040 kg/m³, viscosity 0.0018 Pa·s and bulk modulus $K_f = 2.25$ Gpa.

Numerical Experiments.III

Example 1:

- We used a 100x100 mesh in all examples where the fractures are modeled as boundary conditions. When fractures were modeled as thin layers, a 109x100 non-uniform mesh was used.
- Fracture aperture $h^{(f)} = 1$ mm.
- Frequency 60 Hz.

Numerical Experiments.IV

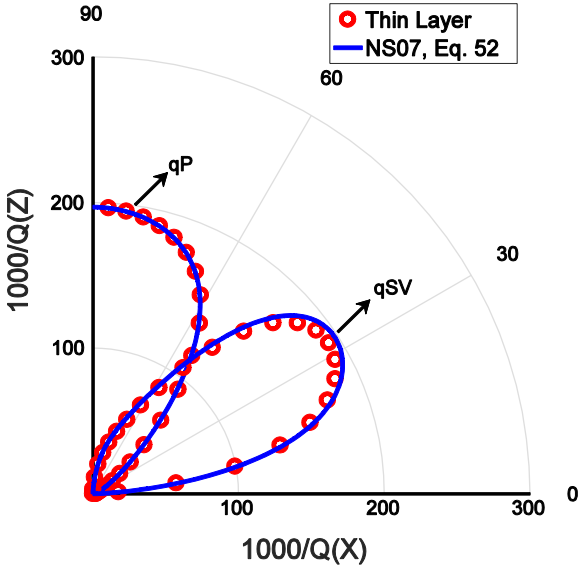

Dissipation Factor

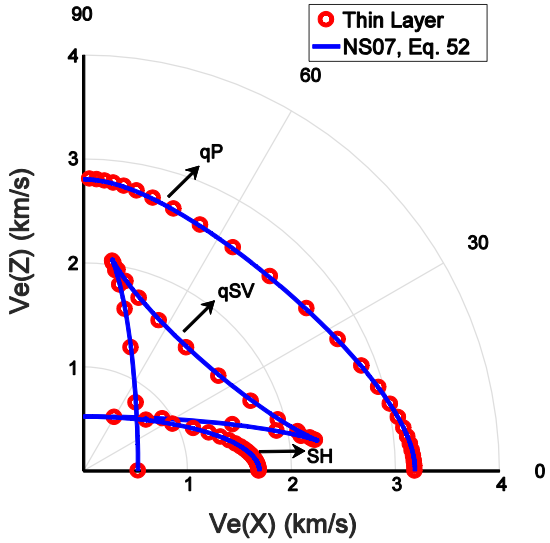

Energy Velocity

Numerical Experiments.V

Example 2:

- The saturating fluid in the background is gas with density ρ_f = 500 kg/m³, viscosity η = 0.00002 Pa·s and bulk modulus K_f = 0.025 GPa. The fractures are saturated with brine.
- Fracture aperture $h^{(f)}$ = 5 cm and 5 mm.
- Frequency 60 Hz.

Numerical Experiments.VI

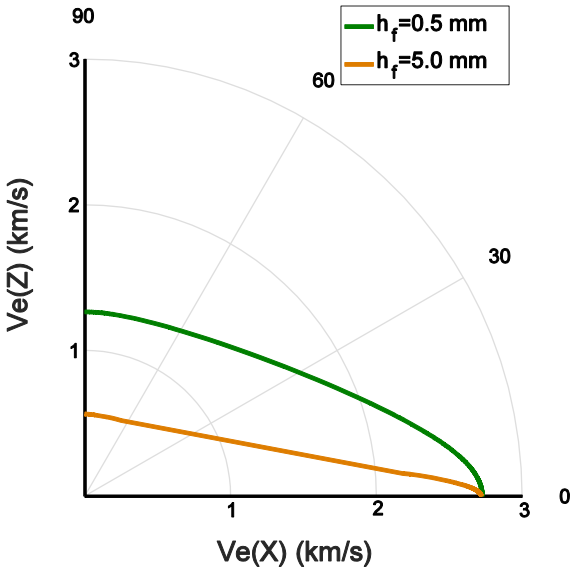

Energy Velocity qP-waves

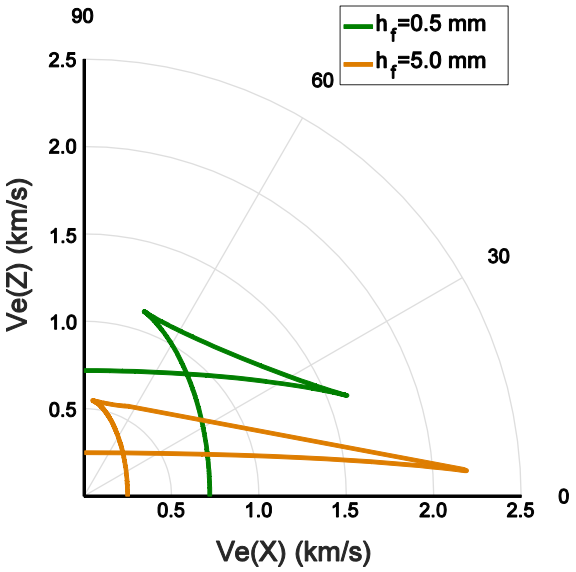

Energy Velocity qSV-waves

Energy velocity anisotropy increases as fracture aperture increases. Also, velocity decreases for waves arriving normally to the fracture layering

SEG
INTERNATIONAL EXPOSITION AND 87TH ANNUAL MEETING
HOUSTON·TEXAS
24-29 SEPTEMBER 2017

Numerical Experiments.VII

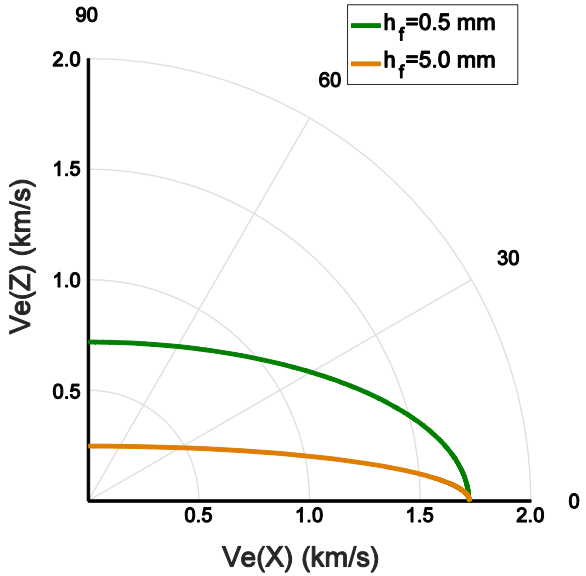

Energy Velocity SH-waves

Numerical Experiments.VIII

Example 3:

- This experiment performs a sensibility analysis to study velocity variations in fractured poroelastic samples due to changes in volume fractions of Material 3 in the samples (background and fractures).
- Both background and fractures are brine saturated.
- Fracture aperture $h^{(f)}$ = 1 mm, frequency 60 Hz.

Numerical Experiments.IX

- Porosity spatial distribution in the background of the fractal sample for the case of 10% volumen fraction of Material 3.
- In this sample both background and fracture properties vary in fractal form.

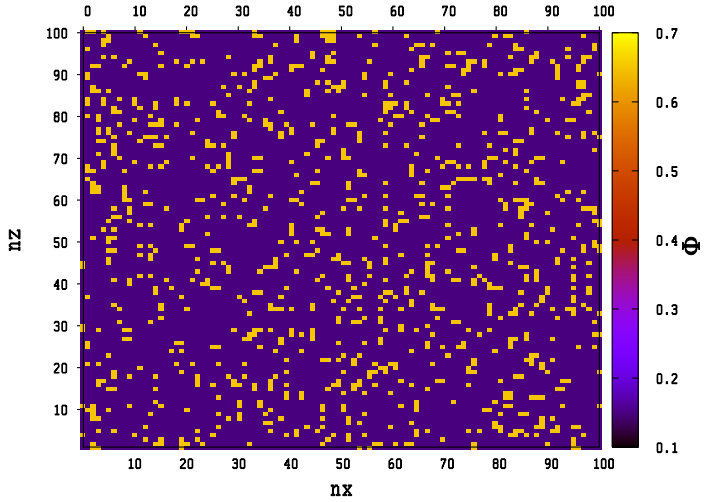

Numerical Experiments.X

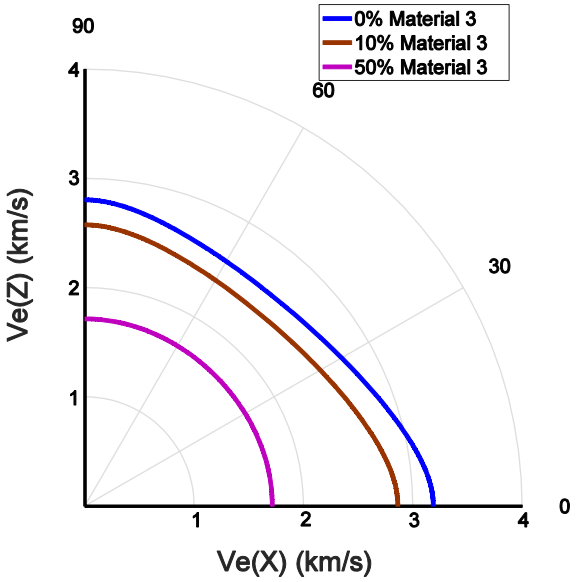

Energy Velocity qP-waves

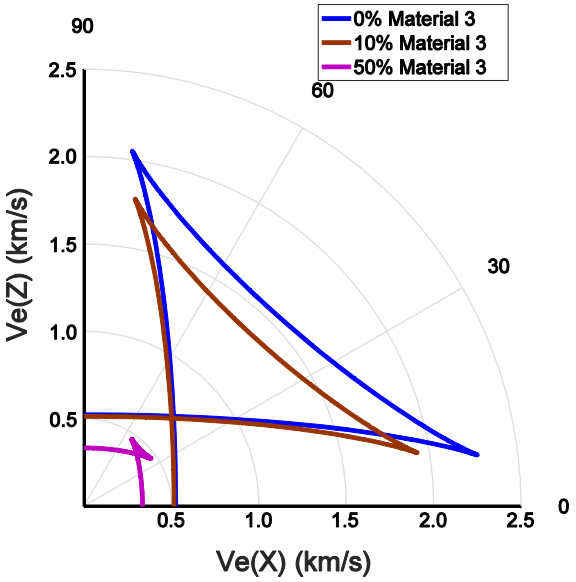

Energy Velocity qSV-waves

Energy velocity anisotropy decreases as proportion of Material 3 increases.

SEG INTERNATIONAL EXPOSITION AND 87TH ANNUAL MEETING
HOUSTON·TEXAS
24-29 SEPTEMBER 2017

Numerical Experiments.XI

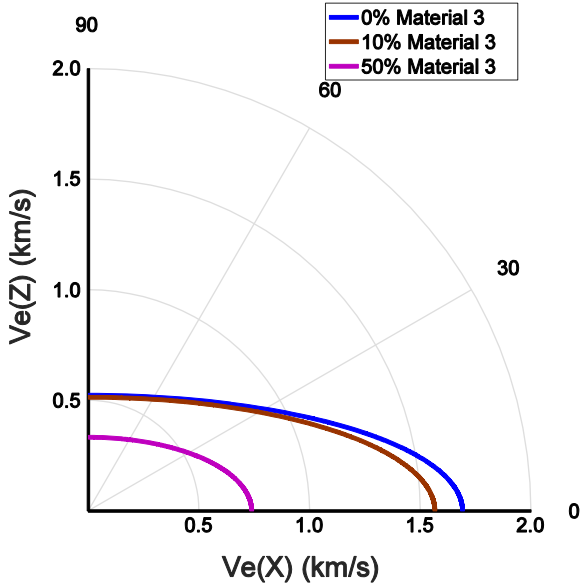

Energy Velocity SH-waves

Energy velocity of SH waves remains large even for large proportions of Material 3.

Conclusions.I

- The procedure was first validated comparing the results with those obtained for fractures modeled as fine layers.
- In all cases, the experiments show that fractures induce strong velocity anisotropy.
- Larges increase in anisotropy was observed for large increases in the openings of the fractures.

Conclusions.II

- Energy velocities for qP and qSV waves were observed to decrease as the volume fraction of the fractal heterogeneities increase, with these two waves tending to behave isotropically.
- SH energy velocities remained anisotropic even for large volume fractions of fractal heterogeneities.

Conclusions.III

- The results of the last two experiments suggest that this FE procedure may become a useful tool to study variations in energy velocities in hydrocarbon reservoirs subject to hydraulic fracturing.

THANKS FOR YOUR ATTENTION !!!!!